SUPPLEMENTAL MATERIAL

Supplemental Figures S1 and S2 (see below) show that in ClC-2 the $G_{norm}([H^+]_o)$ increased as the $[H^+]_o$ increased, reached a maximum when $[H^+]_o$ was $10^{-6.4}$ M but with further increases in $[H^+]_o$ the G_{norm} decreased. This behaviour indicates protonation of at least 2 sites, S1 and S2. Protonation of S1 causes an increase in G_{norm} while protonation of S2 decreases G_{norm}. Therefore, in order to test if external H^+ stabilizes the open state in ClC-2, two schemes (I and II) were built to describe the behaviour of the fast gate (S1) under different external $[H^+]_o$. If ClC-2 gating follows Scheme I, then the open probability is given by:

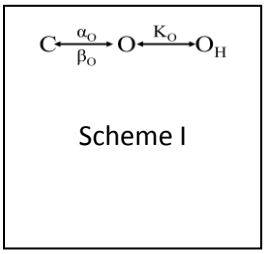

Scheme I

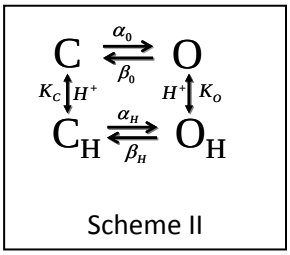

Scheme II

$$P_{OI} = \frac{1+\frac{[H^+]_O}{K_O}}{1+\frac{\beta_O}{\alpha_O}+\frac{[H^+]_O}{K_O}} \quad \text{Equation 1}$$

where K_O is the equilibrium constant of protonation for open channels and β_O/α_O is the ratio of rate constants for the C ↔ O transition. To account for the decrease in G_{norm} due to protonation of S2 at very acidic pH_O (<6.4) the function describing G_{norm} was multiplied by $1/(1+([H^+]_O/K_2)^{n2})$. K_2 and n_2 are the equilibrium constant for S2 protonation and the Hill coefficient, respectively. Thus, G_{norm} was given by:

$$G_{norm} = P_{OI}\frac{1}{1+\left(\frac{[H^+]_0}{K_2}\right)^{n_2}} \quad \text{Equation 2}$$

Similarly, if the gating behaves as described in Scheme II, then the open probability is given by:

$$P_{OII} = \frac{1+\frac{[H^+]_o}{K_O}}{1+\frac{[H^+]_o}{K_O}+\left(\frac{\beta_O}{\alpha_O}\right)\left(1+\frac{[H^+]_o}{K_C}\right)} \quad \text{Equation 3}$$

where K_O and K_C are the equilibrium constants of protonation for open and closed channels, respectively. β_O/α_O is the ratio of rate constants for the C ↔ O transition. To account for the decrease in G_{norm} at acidic pH_O (<6.4) due to protonation of S2, the function describing P_{OII} was multiplied by $1/(1+([H^+]_O/K_2)^{n2})$, where K_2 and n_2 are the equilibrium constant for S2 protonation and the Hill coefficient, respectively. Thus, G_{norm} was given by:

$$G_{norm} = P_{OII} \frac{1}{1+\left(\frac{[H^+]_0}{K_2}\right)^{n_2}}$$ Equation 4

Supplemental Figure S 1. Scheme I explains $G_{norm}([H^+]_o)$ and $G_{norm}(V_m)$ but not $\tau_c(pH_o)$. **A:** G_{norm} vs $[H^+]_o$ curves at each V_m were constructed using the interpolated values obtained from fitting $G_{norm}(V_m)$ curves with a Boltzmann function (Figure 3B). V_m= -20 to -200 mV in 20 mV increments. **B:** Corrected G_{norm} vs V_m curves at $[H^+]_o = 10^{-9.1}$ (▼), $10^{-8.4}$ (▲), $10^{-7.3}$ (●), and $10^{-6.4}$M (■). Continuous lines through data in A and B are fits with Equations 2 and 1, respectively. To fit data shown in B with equation 1 we assumed that β_O/α_O varied in an exponential fashion with voltage, as proposed by the rate theory. **C:** Lack of V_m-dependence of pK. These pK values were obtained from fitting data shown in panel A (open circles) or from fitting data shown in panel B (black line). Closed circles are pK values for protonation of S2. **D:** Ratio of rate constants describing the transition C to O according to Scheme I. Closed symbols are values obtained from fitting data shown in panel A while continuous lines are the values obtained from fitting data shown in panel B. **E:** Equation 5 (continuous line) for τ_c according to Scheme I did not explain the $\tau_c(pH_o)$ data.

Supplemental Figure S 2. Scheme II predicts V_m-independent protonation and V_m-dependent chlorination. **A:** G_{norm} vs $[H^+]_o$ curves at each V_m were constructed as described in Figure S1A. **B:** Corrected G_{norm} vs V_m curves at $[H^+]_o = 10^{-9.1}$ (▼), $10^{-8.4}$ (▲), $10^{-7.3}$ (●), and $10^{-6.4}$M (■). Continuous lines through data in panels A and B are fits with Equations 4 and 3, respectively. To fit data shown in B with equation 3 we assumed that β_O/α_O varied in an exponential fashion with voltage, as proposed by the rate theory. **C:** Lack of V_m-dependence of pK. pK values were obtained from fitting data shown in panel A (open circles) or from fitting data shown in panel B (black line). Closed circles are pK values for protonation of S2. **D:** Ratio of rate constants for the transition C to O according to Scheme II. Closed symbols are values obtained from fitting data shown in panel A, while continuous lines are values obtained from fitting data shown in panel B.

Supplemental Figure S 3. Simulations of ClC-2 gating according to Model 1 based on Scheme I. **A:** Complete Model 1 depicting an empty pore (lower row) or a pore occupied by Cl^- (upper row). The protopore gate (red sphere) is in the closed position (left column) or the open position (middle and right columns). An open protopore gate can be stabilized by protonation from the extracellular side (right column). Transitions between states are controlled by rated constants weighed by allosteric factors (f) that account for the presence of Cl^- in the pore. K^H_O, the equilibrium constant of protonation, was considered V_m-independent as suggested by analysis of the data using Scheme I (Figure S1). **B:** Simulations of $I_{Cl}(t)$ from -200 to -60 mV according to protocol shown in the upper part. **C:** Simulations of the effects of $[Cl^-]_i$ on the time course of G_{norm} (upper half of the panel). As previously reported τ_c was decreased by increasing $[Cl^-]_i$ (Sanchez-Rodriguez et al., 2010); this effect is shown in lower half of this panel. **D:** Simulations of the effects of $[Cl^-]_o$ on the time course of G_{norm} (upper half) and on τ_c (lower half). As previously reported, increasing $[Cl^-]_o$ has no effect on ClC-2 gating (Sanchez-Rodriguez et al., 2010).

Supplemental Figure S 4. Model 1 reproduced the $[H^+]_o$-, $[Cl^-]_i$- and $[Cl^-]_o$-dependency of $G_{norm}(V_m)$. $G_{norm}(V_m)$ curves were simulated according to Model 1 under different $[H^+]_o$ (panel A), different $[Cl^-]_i$ (panel B), and different $[Cl^-]_o$ (panel C). Numbers in each plot correspond to M concentrations of these ions.

Supplemental Figure S 5. Model 1 did not reproduce the $[H^+]_o$ dependence of τ_c. **A:** G_{norm} at -180 mV and at +60 mV were simulated at $[H^+]_o$ ranging between 10^{-10} to $10^{-6.4}$ M. Note that the closing rate became slower as $[H^+]_o$ increased. **B:** t_c as a function of $[H^+]_o$. Note that contrary to the experimental results (Figure 5G), model 1 predicts a non saturable time constant.

Supplemental Table 1. Models that favour opening by protonation of closed channels. The dissociation constant is denoted by $K_H=k_-/k_+$.

Scheme	**Open probability**	**Closing time constant**

$C \overset{K_H}{\leftrightarrow} O_H$	$\frac{1}{1+K_H/[H]}$	$\approx \frac{1}{k_{-1}}$
$C \overset{K_H}{\leftrightarrow} C_H \underset{\beta}{\overset{\alpha}{\rightleftarrows}} O_H$	$\frac{\alpha}{\alpha+\beta+\beta(K_H/[H])}$	$\approx \frac{1}{\beta}$
$C \overset{K_H}{\leftrightarrow} O_{1H} \underset{\beta}{\overset{\alpha}{\rightleftarrows}} O_{2H}$	$\frac{\alpha+\beta}{\alpha+\beta+\beta(K_H/[H])}$	$\approx 2/(k_- + \sqrt{((k_-)^2 - 4(k_- * \beta))}$ $\approx 2/(k_- - \sqrt{((k_-)^2 - 4(k_- * \beta))}$
$C \overset{K_{Cl}}{\leftrightarrow} C^{Cl} \overset{K_H}{\leftrightarrow} C_H^{Cl} \underset{\beta}{\overset{\alpha}{\rightleftarrows}} O_H^{Cl}$	$\frac{\alpha}{\alpha+\beta+\beta(K_H/[H])(1+K_{Cl}/[Cl^-])}$	$\approx \frac{1}{\beta}$

Figure S1

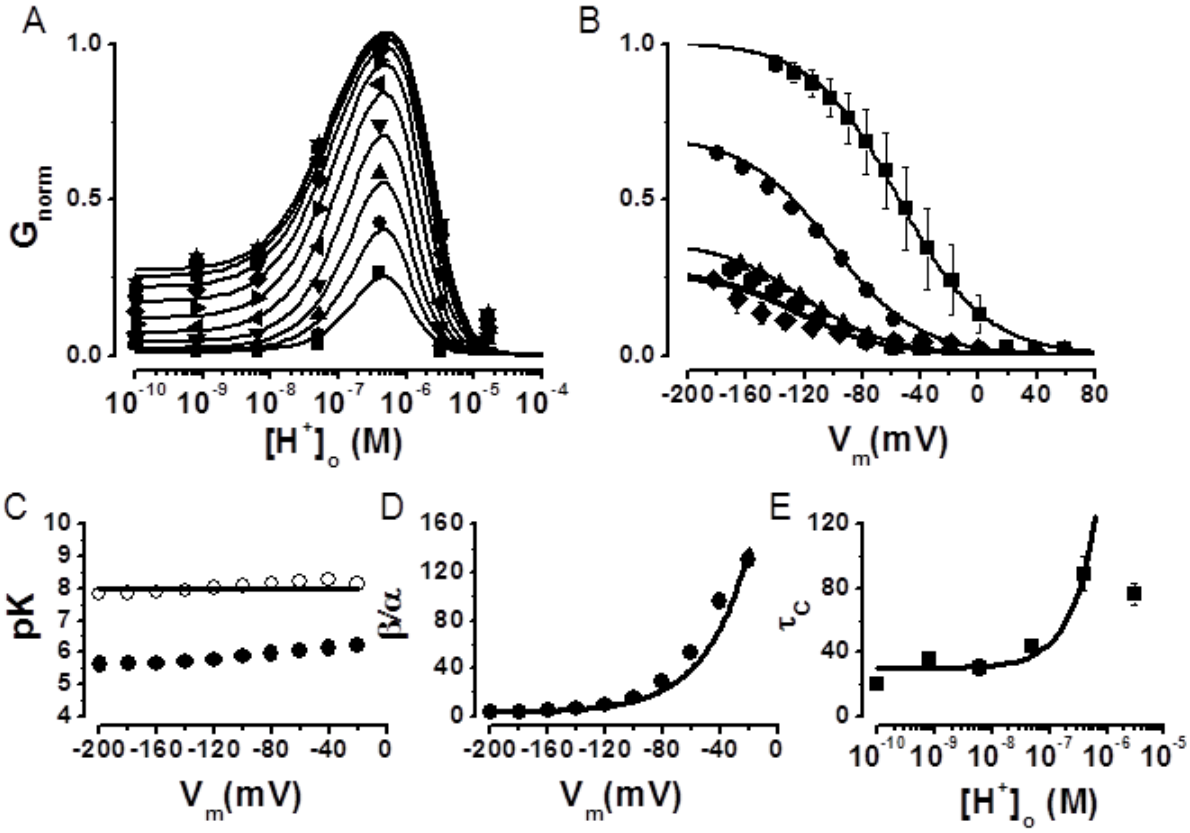

Figure S2

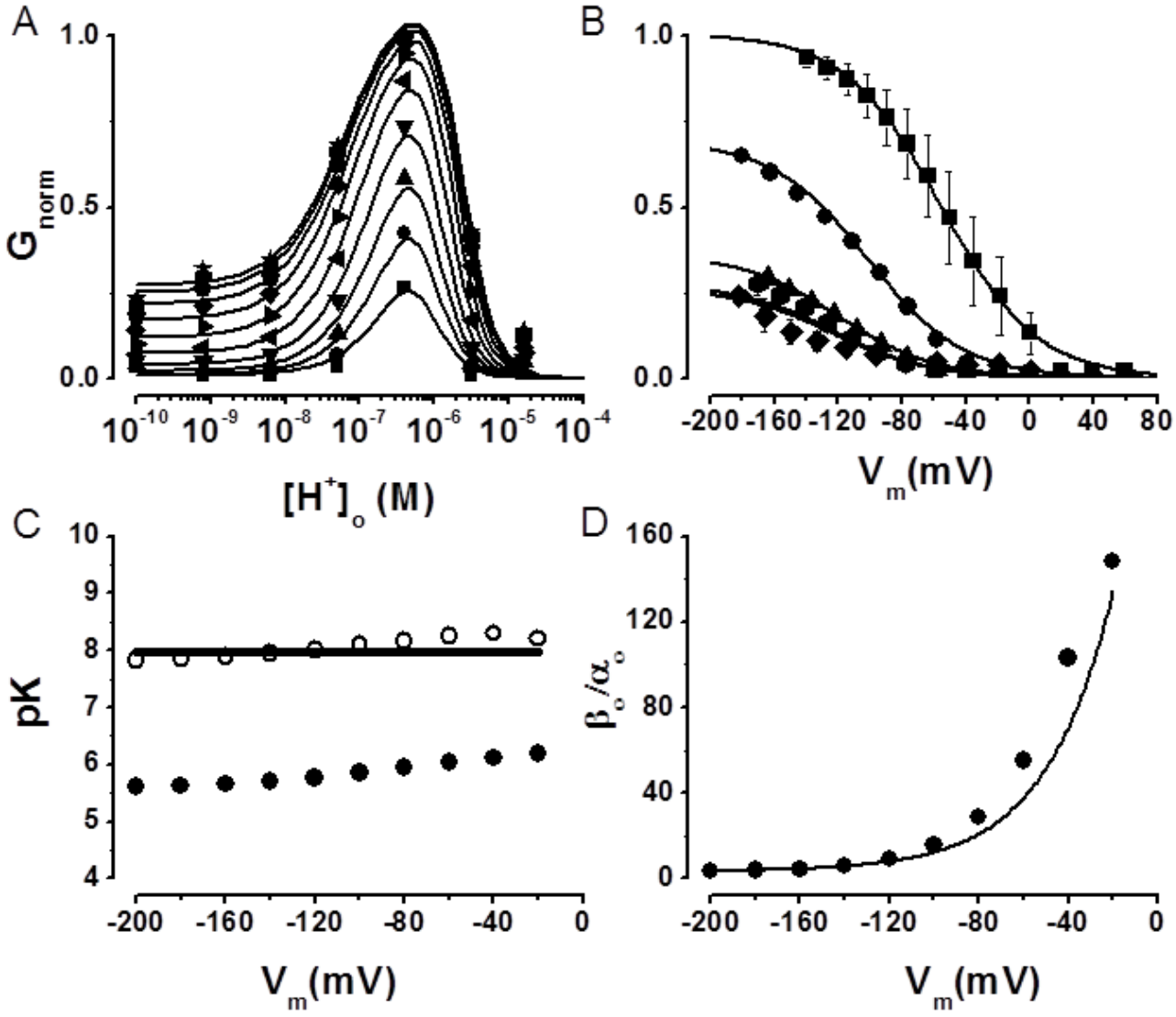

Figure S3

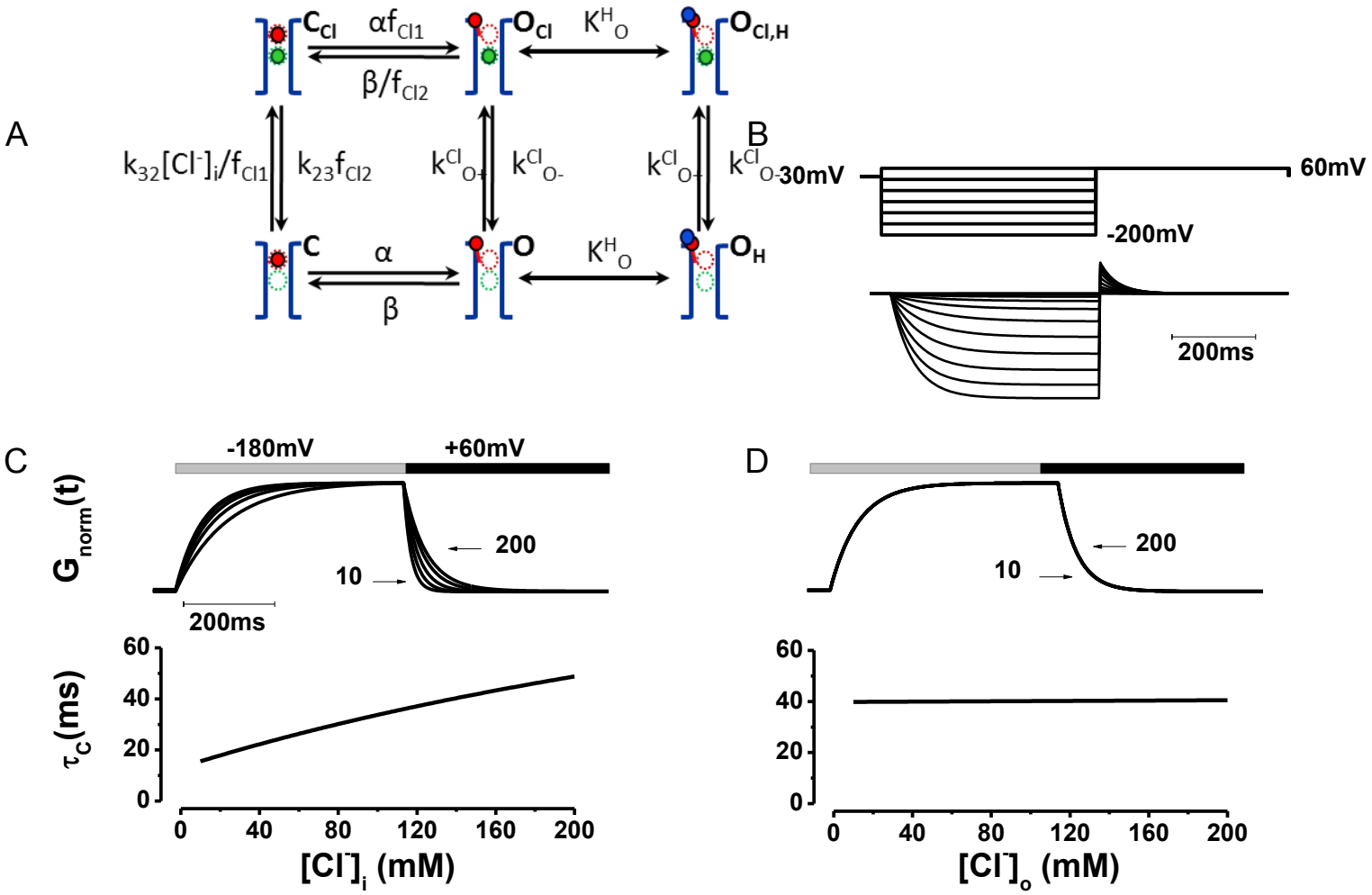
A
B
C
D
-30mV
60mV
-200mV
200ms
-180mV
+60mV
200
10
200ms
[Cl-]i (mM)
[Cl-]o (mM)

Fiugre S4

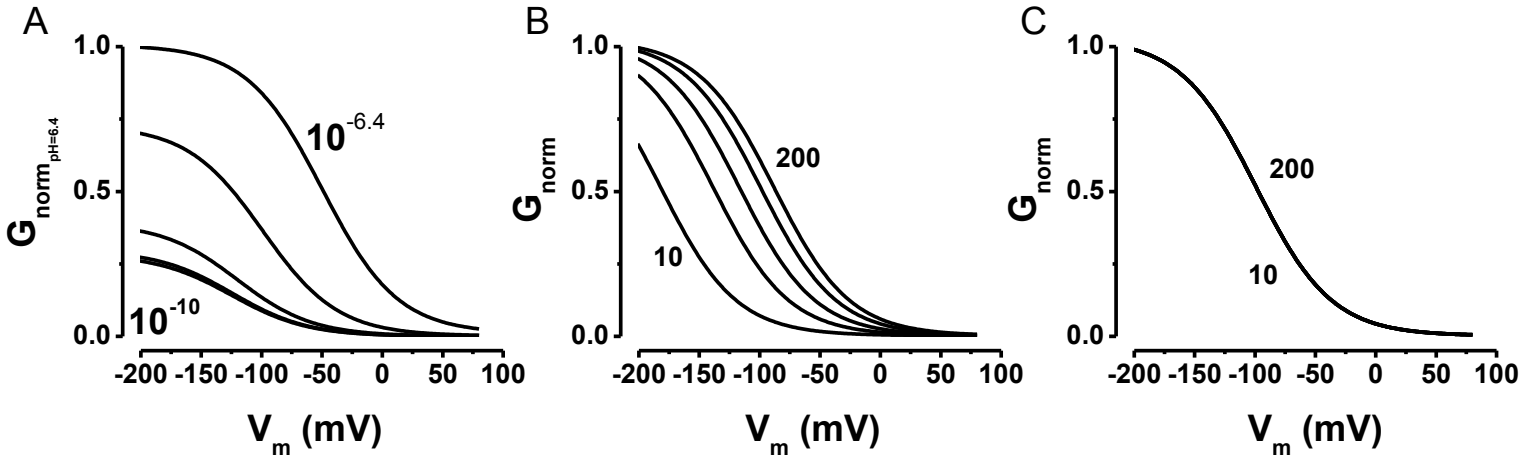
A
B
C
1.0
0.5
0.0
$G_{norm_{pH=6.4}}$
G_{norm}
$10^{-6.4}$
10^{-10}
200
10
-200 -150 -100 -50 0 50 100
V_m (mV)

Figure S5

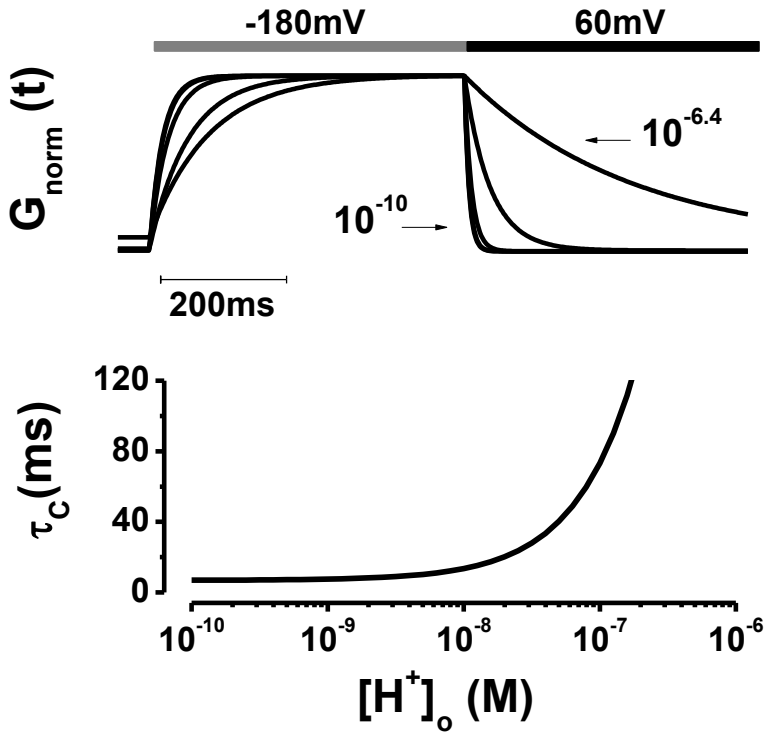
-180mV
60mV
G_{norm} (t)
$10^{-6.4}$
10^{-10}
200ms
τ_c(ms)
120
80
40
0
10^{-10}
10^{-9}
10^{-8}
10^{-7}
10^{-6}
$[H^+]_o$ (M)